Regular Article

Printed circuit heat exchangers and fast neutron radiography

B. Vrban[a] , Š. Čerba, J. Lüley, V. Filová, and V. Nečas

Faculty of Electrical Engineering and Information Technology, Institute of Nuclear and Physical Engineering, Slovak University of Technology in Bratislava, Ilkovičova 3, Bratislava, Slovakia

Abstract Non-destructive testing is capable of detecting defects of important components, where a failure could pose a significant hazard and cause severe economic losses. Currently, imaging techniques utilizing gamma or X-ray sources are mainly used and allow to examine of devices ranging in size from units to tens of centimetres, but for industrial-sized large components, these methods usually fail. The utilization of fast neutrons in radiography is a promising alternative, especially for industrial applications. Currently, due to the higher neutron-matter interaction probabilities, most neutron-imaging systems use thermal neutrons originating from research reactors. Due to the intention of on-site inspection of revealing the possible ruptures and failures, this option is not applicable. The paper presents the newly developed neutronic models of printed circuit heat exchangers where the specific ruptures are defined. Next, neutron transport simulations are performed to investigate the different irradiation geometries, various neutron sources, and backfill materials to access the principal detectability of these ruptures in the industrial environment. Finally, conclusions are drawn, and the best backfill material and neutron source are identified in the simplified model.
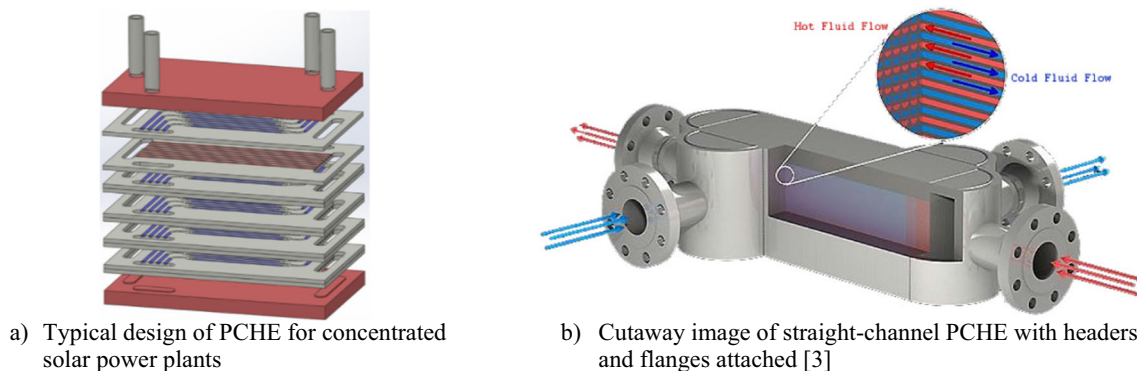
1 Introduction

Non-destructive analysis (NDA) is an important technique for ensuring the integrity of critical components [1]. These methods generally allow testing of the material, without its damage, or with a breach so small, that its functional properties are maintained. In particular, nuclear systems that contain the primary coolant need to be checked when manufacturing and are thoroughly inspected during shutdowns for excessive wear or damage. The estimate of the financial cost of one-day downtime of Slovak NPP Mochovce (1 reactor, 505 MWe, price of generated MWh in early 2022 = 61.25 €) is approx. 740 k€. To reduce the time and cost associated with the maintenance tasks of future energy systems, technicians need to quickly identify potential defects by non-destructive techniques.

One of the most challenging large industrial components is the printed circuit heat exchanger (PCHE), which is one of the compact new-class heat exchangers [2] that can sustain high-pressure differences between primary and secondary coolant sides, see Fig. 1.
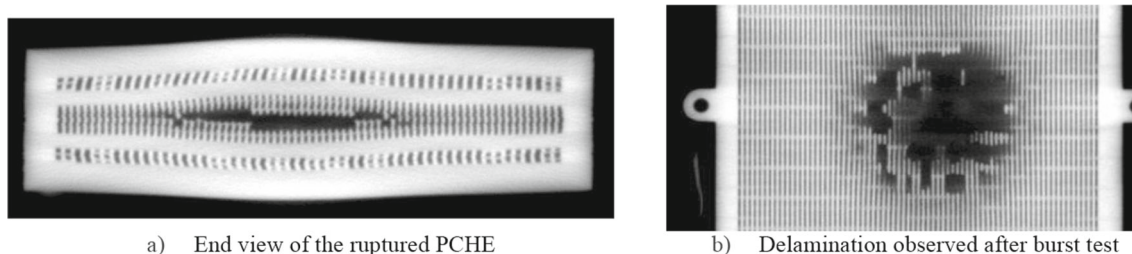
These exchangers are up to 85% smaller and lighter than traditional technologies such as shell and tube heat exchangers [4]. This reduction in unit size can lead to significant savings in structural costs due to the elimination of excess pipework, frames, and associated equipment. The PCHE [5] is characterized by high surface area density while having high thermal efficiency of up to 98% [6]. The design life is approx. 60 years, which is comparable with nowadays lifespan of a nuclear reactor. The limitations are the same as those of plate-fin heat exchangers, with cleaning virtually impossible in the tiny fluid passages, and design-code issues, with no approved material certified to be used in nuclear available. These exchangers are assumed to be implemented also in Generation IV nuclear reactors [2]. Their inspection during the downtimes, especially for the systems utilizing reactive sodium as a coolant, will become a crucial operation affecting nuclear safety. Figure 2 shows examples of the ruptured PCHE which need to be prevented and detected at their early stages. The dark area shows where some of the channel "grid" has been torn away from the original plate and remains diffusion bonded to the adjacent plate.

Printed circuit heat exchangers have channels, which are far too small to allow for visual inspection and

[a] e-mail: branislav.vrban@stuba.sk (corresponding author)

1646

Eur. Phys. J. Spec. Top. (2023) 232:1645–1656

a) Typical design of PCHE for concentrated solar power plants

b) Cutaway image of straight-channel PCHE with headers and flanges attached [3]

Fig. 1 Typical designs of PCHE for various applications

a) End view of the ruptured PCHE

b) Delamination observed after burst test

Fig. 2 Example of possible ruptures of PCHE [3]

dense enough to severely limit the ultrasonic or X-ray imaging capability of the internal geometry. One of the evolving methods of NDA is neutron radiography [7, 8], which uses neutrons produced by subcritical assemblies, nuclear reactors, or accelerators to penetrate dense objects. Neutron radiography has its benefits. Neutrons easily pass-through metals, unlike X-rays which are scattered or absorbed by the electrons of high Z elements such as iron, nickel, and chromium [9]. Moreover, various materials with high absorption cross-sections can be used to backfill PCHE channels to ease the detection of possible damages and defects.

Several scientific problems [10] need to be addressed and solved to allow on-site fast neutron radiography of large components. The first challenge lies in the neutron statistics driven by the source strength of fast neutrons and a large amount of dense material between the source and detector. The number of neutrons reaching the detector has a direct impact on the ability to detect cracks and ruptures of small size. Next, on the detector side, the scintillator converting neutrons to photons need to be optimized to find the best contrast and suitable spatial resolution. The request for improved spatial resolution then interferes with the decreased exposure time. In the case of semiconductor imaging detectors based on Timepix read-out, its enhancement for improved neutron radiography with fast neutrons utilizing the High-Density PolyEthylene (HDPE) layer is under development at STU. In addition, the design of the collimator influences the beam divergence, which might introduce geometric unsharpness and might limit the detectability of ruptures. Moreover, the appropriate reconstruction software needs to be implemented.

1.1 Applications of printed circuit heat exchanger technology

In terms of non-nuclear applications, PCHE is foreseen to be used in concentrated solar power (CSP) plants, offshore oil and gas processing stations, or exhaust waste recovery systems. CSP system generates solar power by using mirrors or lenses to concentrate a large area of sunlight into a receiver transforming this energy into electricity. By operating CSP plants at high temperatures (up to 750 °C [11]), the plant efficiency can be increased by using a compact design leading to lower levelized costs of electricity. One of the key components ensuring these technical features is the heat exchanger that can transfer heat from the medium used to store the sun's energy (e.g., molten salt) to a compressible fluid or gas (CO_2). From the cost perspective, it is advantageous to use a heat exchanger design that has small channels so that the total force applied by the inside medium on the walls of the channel is small even in case of high temperatures and pressures. If the total force is reduced, less material is required leading to lower total fabrication prices. PCHE is expected to be used to transfer thermal energy from the primary molten salt to the secondary CO_2.

In terms of nuclear applications, the situation is similar. Extensive activities for small or microreactors have enabled a new series of Generation IV nuclear reactors that improve the economics and safety of nuclear reactors and reduce radioactive waste. In this regard, Sodium-cooled Fast Reactors (SFRs) have been highlighted for their advantages in improving uranium utilization and disposal of high radioactive waste by

recycling spent nuclear fuel. One of the most promising conceptual designs of SFR is the Korea Advanced Liquid Metal Reactor (KALIMER) with a capacity of 600 MWe. Because of water-sodium reactions in SFR, the use of the Rankine cycle with the highest efficiency is limited, a substitute working fluid is pursued for ensuring safety and efficiency simultaneously, such as carbon dioxide or nitrogen. Based on the evaluation of the working fluid characteristics, various cycle layouts have been proposed by KAERI. The Brayton cycle with CO_2 or N_2 has been found as the most promising solution. Each medium has pros and cons, CO_2 has approximately 38% [5] higher efficiency than N_2, however, it is responsive to sodium. The Brayton cycle with N_2 comprises a heater, pre-cooler, compressor, turbine, and recuperator, among which the recuperator has the largest volume (approx. 68% of the total equipment) and heat capacity. In the case of the CO_2 cycle, it is the intermediate heat exchanger designed to transfer the energy from sodium to CO_2. It is obvious that any effort to reduce the plant footprint should focus on the selection of this equipment, PCHE heat exchangers manufactured by chemical etching and diffusion bonding are foreseen for both designs of the KALIMER reactor, as the recuperator or intermediate heat exchanger. The failure of the PCHE channels utilized in the nuclear industry, whether due to production defects or operation conditions, would lead to a significant environmental, social, and financial impact. To minimize the financial burden but also to enhance the safety of these nuclear systems (e.g., reactors) it is clear, that the probability of a PCHE failure should be as low as possible. This can be achieved by applying material diagnostic methods to identify possible manufacturing defects and defects accumulated during the operation. One of the evolving methods of NDA is neutron radiography, which uses neutrons produced by subcritical assemblies, nuclear reactors, radioisotope sources or accelerators to penetrate dense objects.

1.2 Neutron radiography

Intensive research is currently conducted at the level of imaging techniques for in-situ defectoscopy, where gamma or X-ray sources are mainly used. Neutron radiography is one of the most promising methods to use in the evaluation of production defects of PCHE panels and has numerous benefits over conventional X-ray techniques. Neutrons in general pass-through materials that X-rays cannot, whereas X-rays pass through materials that are almost impossible for neutrons. While X-ray and gamma radiography's ability to provide information about low-density materials, especially in the presence of higher-density materials, is very poor, neutron radiography does not suffer from this limitation. When neutrons pass through an object, they provide information about the internal structure of that object. X-rays interact weakly with low atomic number elements (e.g., hydrogen) and strongly with high atomic number elements, such as metals. On the other

hand, while X-rays follow nearly linear attenuation with density, neutrons follow no such trend. Neutrons interact strongly with some very light elements with a low atomic number, such as hydrogen, while easily passing through many of the dense high atomic number elements that would give X-rays pause. Moreover, various materials with high absorption cross-sections can be used to backfill PCHE channels to ease the detection of possible damages and defects. As a result, these two methods both show details that one would overlook if only used a single method. To put the difference between X-rays and neutrons in simple terms, X-rays are good at showing dense materials within light materials [12]. On the other hand, neutrons are good at showing light materials within dense materials (such as a metal object with another substance or empty space inside it), which is exactly the case for the production and operational defects of PCHE systems.

1.2.1 Registering of neutrons

Registering neutrons, the indirectly ionizing particles usually requires neutron conversion to particles detectable by radiation imaging systems. In the case of fast neutrons and semiconductor detectors, an effective conversion reaction is the elastic scattering on light atoms like hydrogen, recoiling its nucleus, the proton. Layers of polyethylene [13–15], paraffine [16] or high-density polyethylene (HDPE) [17, 18] can be used as the coating of the X-ray imaging systems. However, the products of the conversion reaction (protons) are scattered under various angles, which deteriorates the quality of the image, especially in the case of high energies of particles. The higher energy the conversion products receive from neutrons, the larger deviation between the position of particle registration and the real position of neutron primary interaction will be. Recent imaging systems developed for X-ray imaging do not have to solve this problem, as the photons lose their energy in single interaction contrary to protons, which traverse the sensor and deteriorate the space resolution of the system. Hybrid pixel detectors present radiation imaging systems of the newest generation, operating in so-called single particle counting mode, a reading-out signal from every single particle detected. Each sensor pixel is bump-bonded to its own read-out chain on an integrated circuit placed directly beneath the pixel, arranged on one CMOS ASIC (Application Specific Integrated Circuit) or read-out chip. The Timepix read-out chip developed by Medipix2 collaboration [19] contains 256×256 pixels with 55 µm pitch. The problem of traversing protons is solved by various concepts in neutron radiography with Timepix, either by using the microchannel plate [20] or using the MURA mask [16]. However, these solutions do not reach the original space resolution of the system. The development of hybrid pixel detectors based on Timepix read-out chip brought new operating possibilities, which are suitable to significantly eliminate the effect of proton traversing in the sensor. Fortunately, the development of o

read-out chips is ongoing and currently, the Timepix4 read-out chip is awaited. In comparison, to Timepix3, it will exhibit an 8-times better time resolution of 195 ps, which might increase the precision of proton tracking and consequently improve the quality of a final image. The hybrid pixel detectors based on Timepix read-out chips are standardly developed with sensors made from silicon, the most widespread material in electrotechnology. However, for radiation-demanding applications, single-pad detectors from other semiconductor materials with increased radiation stability, like GaAs or SiC [21], emerge. The base material quality is significantly affecting the detector quality and functionality. The SiC radiation detectors show very good energy resolution (like Si detectors) together with high thermal and radiation stability, strongly exceeding standard semiconductor materials. Their drawback is a very high price, due to demanding production technology. The GaAs detectors have radiation stability on the level of SiC detectors but poorer energy resolution and a much more favourable price.

1.2.2 Neutron source

The used source of neutrons is a relevant research topic. Currently, most neutron-imaging systems use research reactors that serve as a source of thermal neutrons. However, research reactors have several disadvantages. Usually, the power and, therefore, the available neutron flux are not high enough and, therefore, achieving a good quality image requires large irradiation times. If the power of the reactor is sufficient, fuel burnup issues may arise. The reactors are large equipment, which cannot be moved, and irradiation (neutron imaging) can be only performed through dedicated channels, which are again limited by the available flux and energy of neutrons. These reactors have also been built (usually decades ago) for dedicated purposes and neutron imaging can be only a side activity with limited time availability. Compared to nuclear reactors, accelerators produce far less radioactive waste and have lower safety and logistical regulatory burdens. These accelerators can be set up to generate neutrons through the DD (deuterium-deuterium), DT (deuterium–tritium) or TT (tritium-tritium) fusion reactions. Each fusion reaction produces well-defined energy of neutrons, which can be precisely set up according to the voltage of the accelerator beam. The emitted energies can be subsequently moderated reflected and collimated using a beam collimator and special materials for a particular purpose.
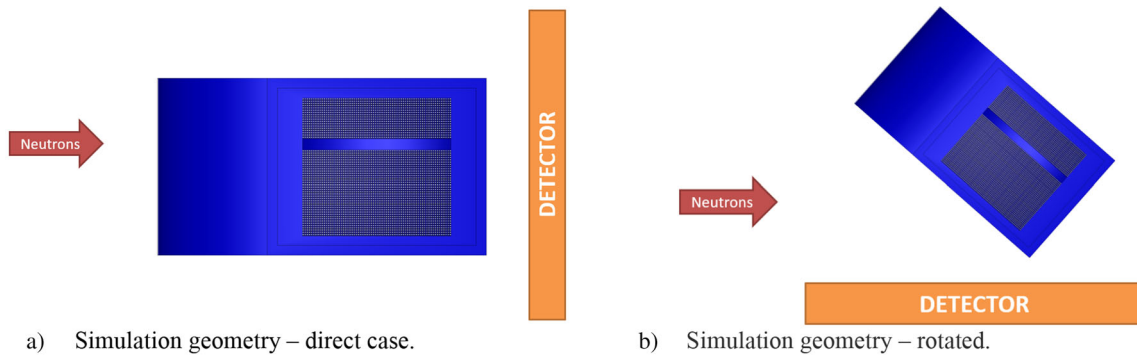
2 Methods and techniques

2.1 SCALE modelling and simulation suite

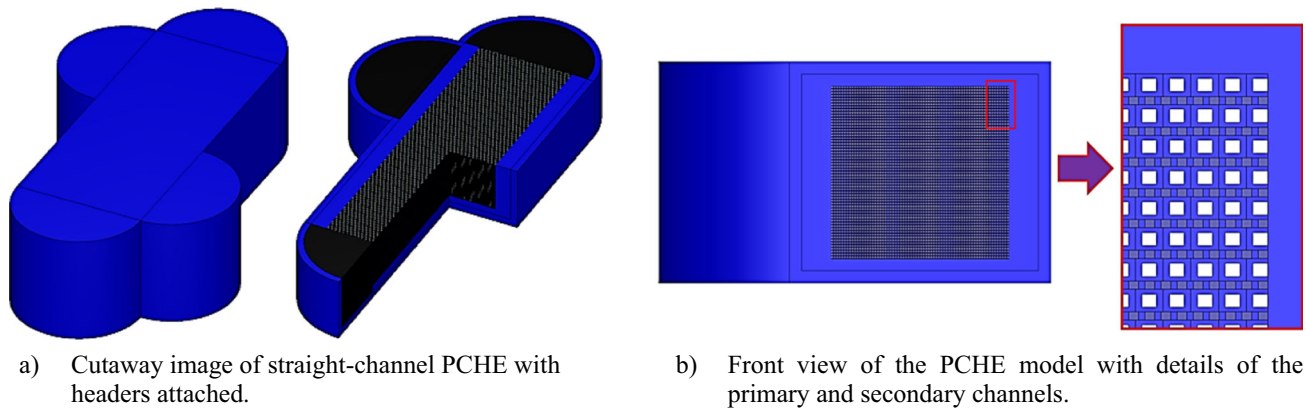An accurate treatment of neutron transport in PCHE characterized by heterogeneous and complex design requires the use of advanced computational tools. The SCALE comprehensive modeling and simulation suite [22] for nuclear safety analysis and design that is developed, maintained, tested, and managed by the Reactor and Nuclear Systems Division (RNSD) of Oak Ridge National Laboratory (ORNL) was chosen to perform the first simulations of fast neutron transport in PCHE. It is worth mentioning that SCALE provides a comprehensive, verified and validated tool set for criticality safety, reactor physics, radiation shielding, radioactive source term characterization, and sensitivity and uncertainty analysis. The sequence MAVRIC, included in the SCALE 6.2.3 code system, was used to perform all simulations presented in the paper. Monaco with Automated Variance Reduction using Importance Calculations (MAVRIC) fixed source radiation transport sequence is designed to apply the multigroup and continuous energy fixed source Monte Carlo code Monaco to solve problems too challenging for standard, unbiased Monte Carlo methods. The intention of the sequence is to calculate fluxes and dose rates with low uncertainties in reasonable times even for deep penetration problems [22]. The forward Monte Carlo transport performed by Monaco code can use either MG or CE cross-section libraries.

For the sake of brevity, just the most important options used in our modelling approach based on our experience from similar calculations related to detector response in VVER-440 core vicinity [23] are discussed here. The coupled continuous neutron-gamma general-purpose library based on ENDF/B-VII.1 was utilized in our simulations. The neutron flux was tallied in the two detector positions (see Fig. 3) where the energy bins were identical to the 199-group VITAMIN-B6 structure except that an additional group has been added to extend the top energy boundary to 20 MeV. The detector behind the PCHE in so-called direct geometry was placed 65 cm from the exchanger core centre, and the shortest distance of the core centre to the detector in rotated geometry was set to 110 cm. Each ideal virtual detector was simulated as a mesh tally comprising 6660 cells with a size of $1 \times 0.5 \times 0.5$ cm (45 pcs in the y-direction and 148 pcs in the z-direction).

The quasi-monoenergetic neutrons used in the simulation were assumed to be generated through the DD (deuterium-deuterium) and DT (deuterium–tritium) fusion reactions. The assumed neutron energies were 2.45 MeV and 14 MeV, where for simplicity the neutron beam was assumed to be perfectly parallel and generated from the 5×5 cm plane. In total 9×10^7 histories of neutrons were simulated without the application of variance reduction techniques, thus giving the total neutron fluence of $3.6 \times 10^7/\text{cm}^2$. In principle, always a pair of two simulation cases were investigated, where the detector response related to the PCHE model without defect was subtracted from the response of the detector related to the PCHE model with specific rupture. The resulting data was visualized by the arbitrary tool.

a)   Simulation geometry – direct case.

b)   Simulation geometry – rotated.

Fig. 3 Definitions of simulation geometries

a)   Cutaway image of straight-channel PCHE with headers attached.

b)   Front view of the PCHE model with details of the primary and secondary channels.

Fig. 4 Simplified model of PCHE developed at STU

2.2 PCHE simplified model

The PCHE is normally constructed from flat metal plates into which fluid flow channels are chemically etched. The plate layout and flow patterns of the cold and hot sides of the exchanger are designed differently, based on the application. In our simplified model, the straight channels of the cold and hot sides are 3 mm wide and 2.5 mm tall (4.5 mm × 4.0 mm) rectangles respectively. The etched plates are then stacked alternately (cold, hot, cold, hot..., cold) and diffusion bonded together. There are 62 cold-side (water) plates and 61 hot-side (sodium) plates in the model. Each cold side plate consists of 120 rectangular channels and 70 above-defined channels can be found in each hot side plate. The total exchanger core dimensions are 80 cm × 67 cm × 200 cm. The core is surrounded by metal walls and headers which distribute the fluids into the exchanger core. In the simplified model, the internal structure of headers was omitted. The casing wall thickness was set to 4.2 cm. Alloy 800H was assumed as the construction material of the PCHE casing and exchanger core. This alloy is an austenitic, heat-resistant nickel–iron–chromium solid solution alloy with controlled levels of carbon, aluminium, titanium, silicon, and manganese and controlled content of (Al + Ti). The simplified model of PCHE developed at STU can be seen in Fig. 4 where to cutaway image

and front view with primary (sodium) and secondary (water) channels are shown.

In parallel to the reference model, the three specific exchanger defects were defined and used in the following simulations. The first simulated defect denoted as a large one and shown in Fig. 5a, is an empty rectangular volume, tall 4.75 cm and in simulation filled by a void. Such an unrealistically large defect was intended to test the overall evaluation methodology and to demonstrate the graphical postprocessing of tallied quantities.
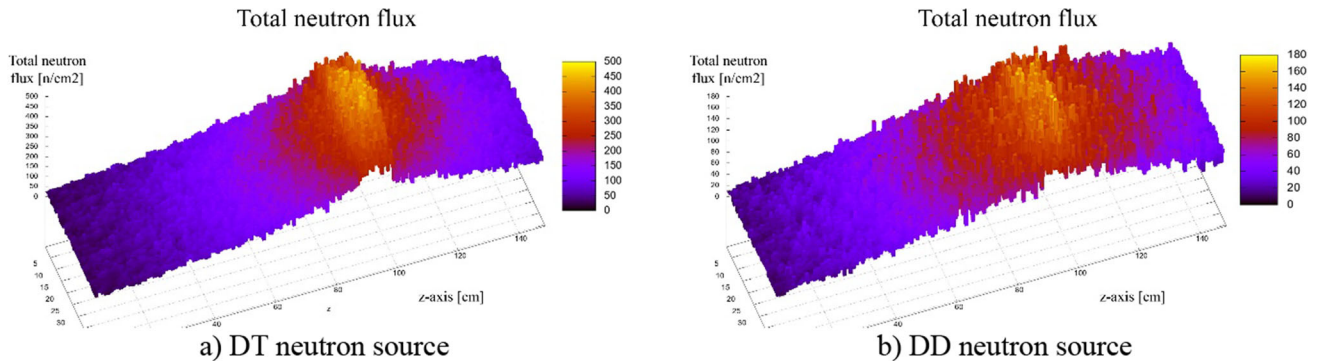
The other two defects visualized in Fig. 5b demonstrate ruptures similar to defects shown in Fig. 3a, where a plate is torn from the adjacent one, and all primary or secondary channels at one horizontal level are merged into one new channel. According to the type of affected channels, these defects are denoted as sodium or water-side defects.

2.3 Simulation scenarios

As shown in the previous section, in total 3 defects were simulated (large, sodium and water) with two geometries (direct and rotated) and two neutron sources (DD and DT). The detector responses were always compared to the reference (without defect) model. The reference parameters of the primary and secondary media assumed during an inspection are the following. The primary sodium with a density of 0.927 g cm^{-3}, 98 °C

a)   Visualization of the large defect.

b)   Definition of the sodium and water channels defects.
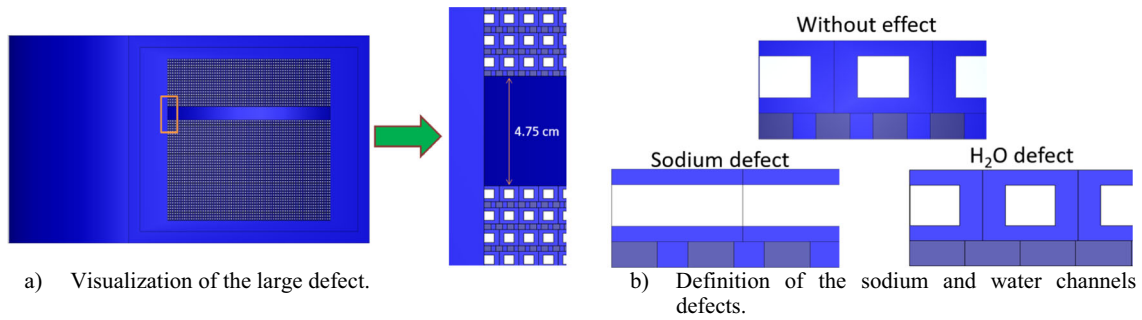
Fig. 5 Defects of PCHE used in the simulation

Fig. 6 Total neutron flux at detector—the large defect—direct geometry

and, atmospheric pressure and the secondary water of the same temperature and pressure with a resulting density of 0.959 g cm^{-3}. In addition, to assess the impact of the different densities of the light nuclide in the backfilling media, the secondary channels were filled by the overheated water steam with a temperature of 550 °C, 20 MPa, and the resulting density of 0.060 g cm^{-3}.

3 Results

The results acquired in the form of ideal detector responses were graphically processed for ease of understanding. Three different approaches were applied to the postprocessing of results. The first type of plot generated shows the subtracted total neutron flux (with defect minus reference case) in each detector cell. The second plot presents the neutron energy spectra on the detector, where the energy group number can be found on the x-axis. The lowest energy group number denotes the neutrons with the highest energies. The third type of plot used displays the sum of total neutron flux responses in detector rows parallel to the defect in the exchanger core.

3.1 Large defect—direct geometry

The first results are devoted to the large defect and direct irradiation geometry. As can be clearly seen from

Fig. 6, both neutron sources (DT and DD) cause significant differences in the total flux at the neutron detector, clearly distinguishing between the part with and without the PCHE rupture. In the case of the DT neutron source, the location of the defect on the detector response is sharper than in the case of the DD source.

A quite interesting response can be found in Fig. 7. There is a higher number of neutrons in almost all energy groups (the final spectra is a subtraction of two simulations). Moreover, in the DT case shown in Fig. 7a, the peak in the fastest energy group can be identified. In the case of the DD neutron source, more neutrons are observable in the lower energy groups, due to their lower starting energy and following scattering reactions.

The responses presented in Fig. 8 are just a special variant of Fig. 6. The idea of summation of responses in detector rows is derived from the principal construction of PCHE and might speed up of detection of possible ruptures. Figure 8 shows the better readability of the plot and easier identification of the rupture positions. It is clear that this approach is not necessary in case of such a large defect, however, may play a role in the case of smaller ruptures.

3.2 Sodium defect—direct geometry

Next, the sodium defect a direct geometry configuration was investigated. The total neutron flux shown in Fig. 9 suggests possible identification of the ruptured plate location by the DT source. In the case of the
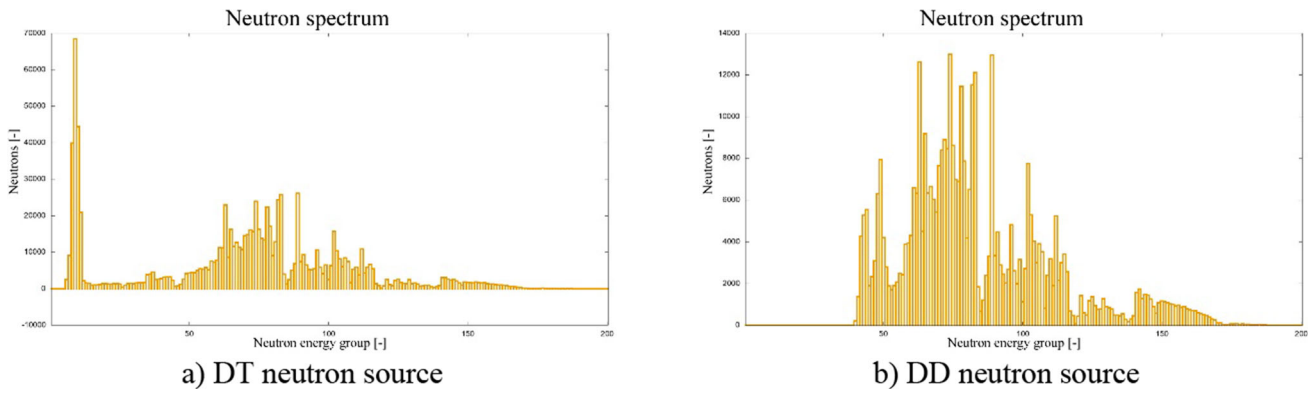
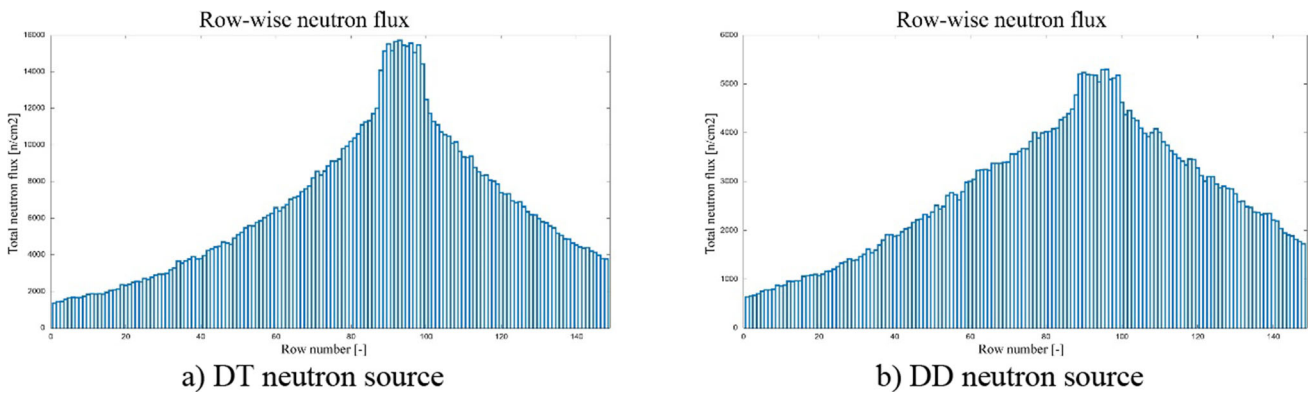**Fig. 7** Neutron spectrum at detector—large defect—direct geometry

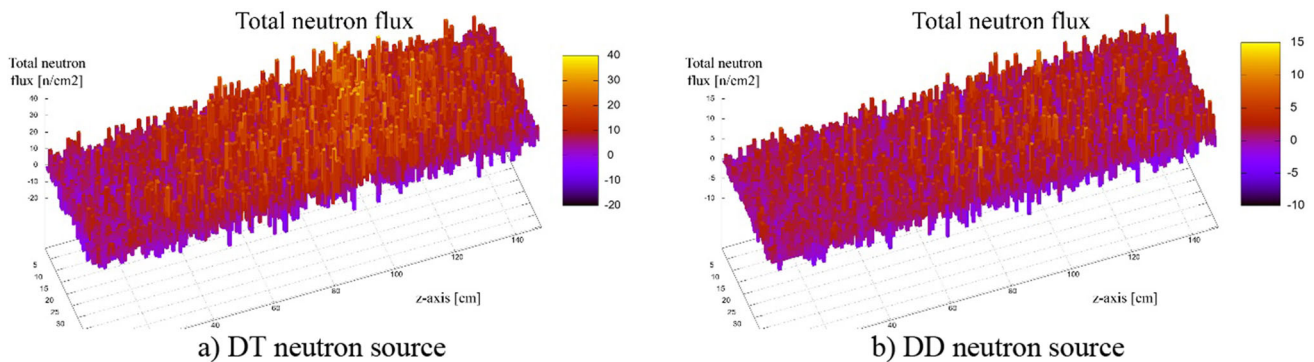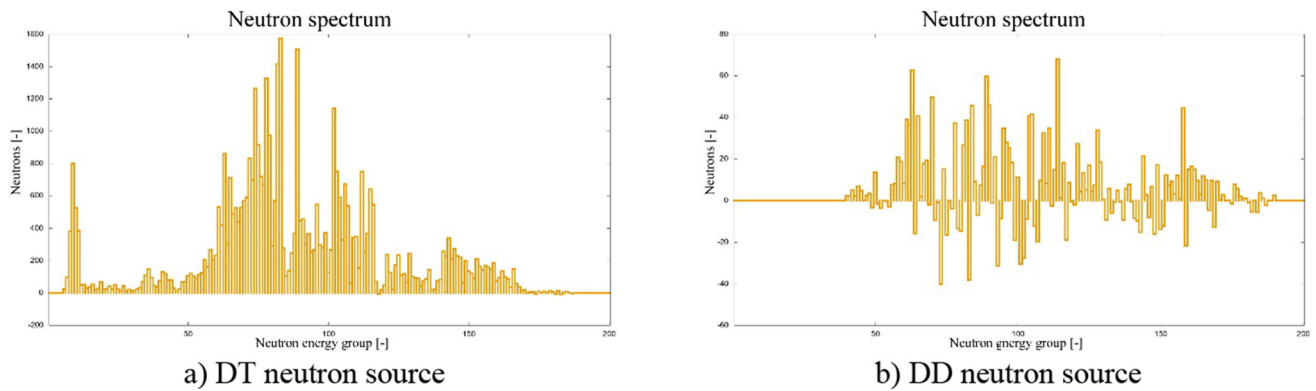**Fig. 8** Row-wise neutron flux at detector—the large defect—direct geometry

Fig. 9 Total neutron flux at detector—the sodium defect—direct geometry

DD neutron source, the response does not point to the defect location.

The previous findings are supported also by Fig. 10, where the neutron spectra (after subtraction) are presented. The DT neutron case clearly shows an excess of neutrons in all energy groups, whereas, in comparison to the large defect case, neutrons moved from the fastest neutron energy groups to the lower energy groups. Anyhow, the neutrons in the fastest groups are still observable. The results acquired in the DD case show a different pattern. There are more neutrons in some energies and fewer neutrons in other energies. If the statistical nature of real neutron measurement is considered in the real case, this pattern of data prevents the successful localization of the rupture in a reasonable time.

The row-wise neutron fluxes presented in Fig. 11 just underline the findings from previous paragraphs. Clearly, in case of sodium rupture, the use of the DT source shows much better performance than the DD source. It seems that under the real measurement conditions, the DD source cannot be successfully used to detect this kind of rupture.

1652

Eur. Phys. J. Spec. Top. (2023) 232:1645–1656

Fig. 10 Neutron spectrum at detector—sodium defect—direct geometry
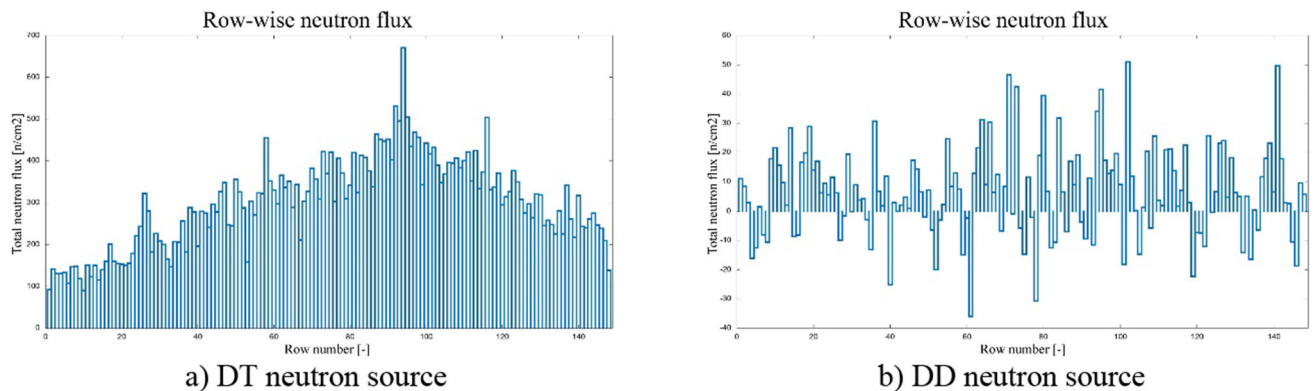
Fig. 11 Row-wise neutron flux at detector—the sodium defect—direct geometry
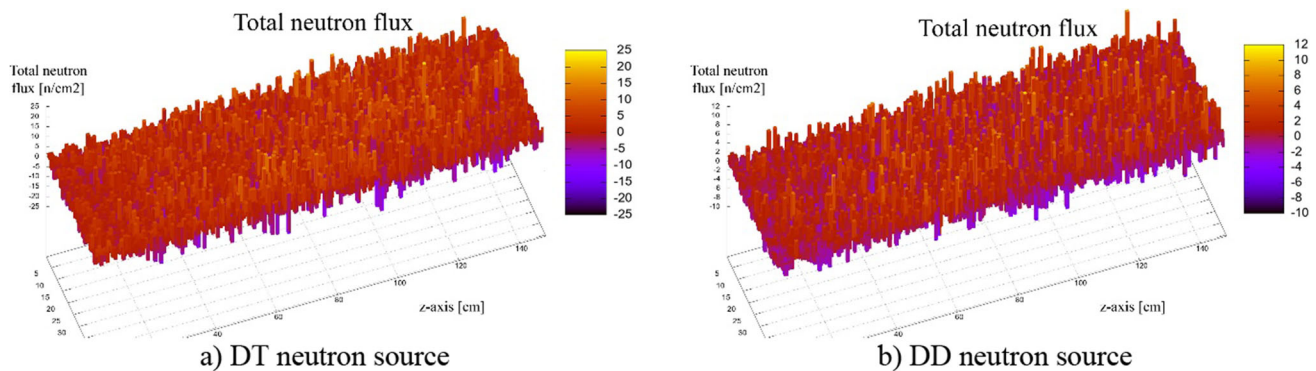
Fig. 12 Total neutron flux at detector—the water defect—direct geometry
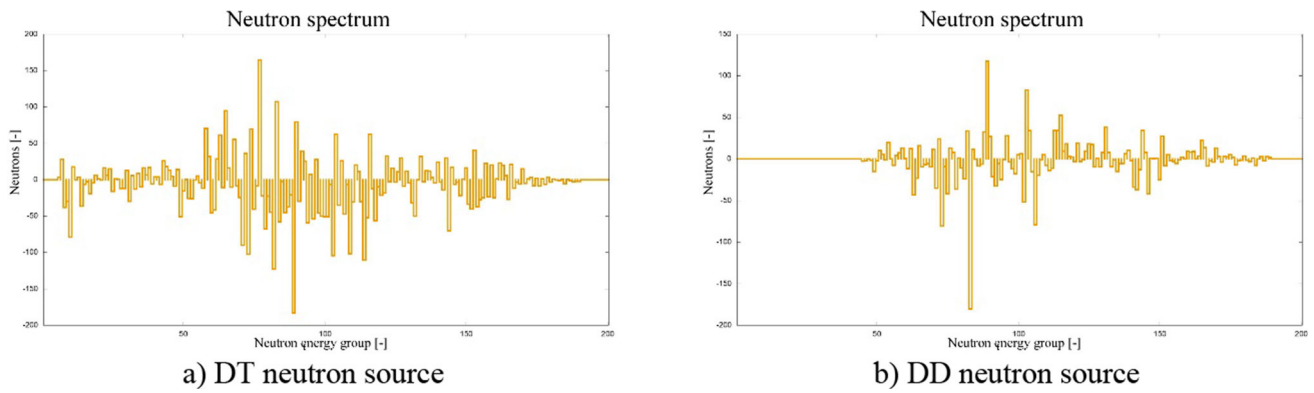
3.3 Water defect—direct geometry

The PCHE secondary side rupture, previously defined as a water defect, was studied using a similar approach as in previous cases and results can be found in the following paragraphs. The results of the total neutron flux (see. Fig. 12) cannot be judged as convincing. No specific pattern can be recognized in either case.

The acquired neutron spectra at detectors (shown in Fig. 13) also do not suggest any clear patterns. Just in the case utilizing the DD neutron source one significant decrease in the number of neutrons between the two simulations can be observed. Theoretically, this isolated decrease of neutrons in the neutron spectra might be principally detectable by resonance activation of foils, however, in practice, we assume this option is complicated and unrealistic in industrial conditions.

The results of row-wise neutron fluxes presented in Fig. 14 just confirm the unfeasibility of water defect detection utilizing DD and DT sources. No pattern can be identified in the DT case. In the DD case, a reader can notice a positive response on the left half of the plot and more negative on the right side. This can be explained by the higher absorption of neutrons with lower energies in the case of simulation with the defect.
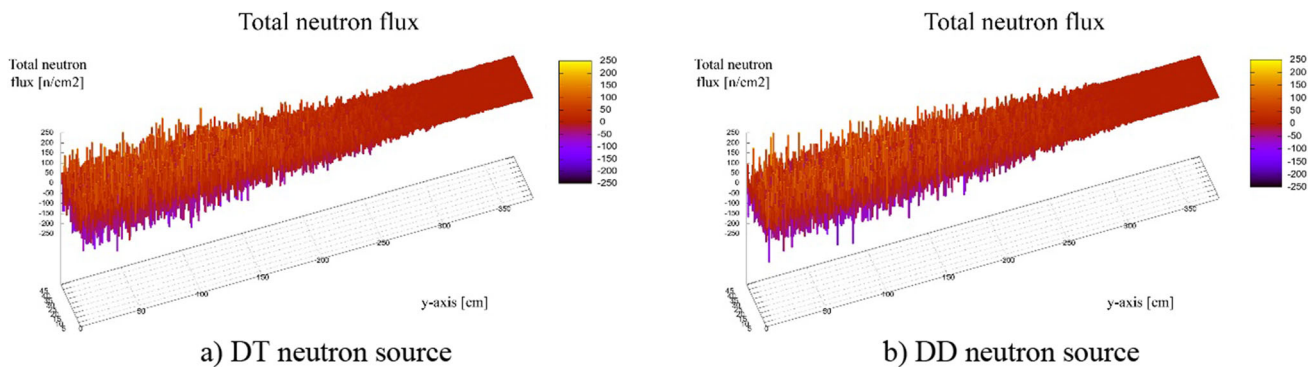
Fig. 13 Neutron spectrum at detector—water—direct geometry
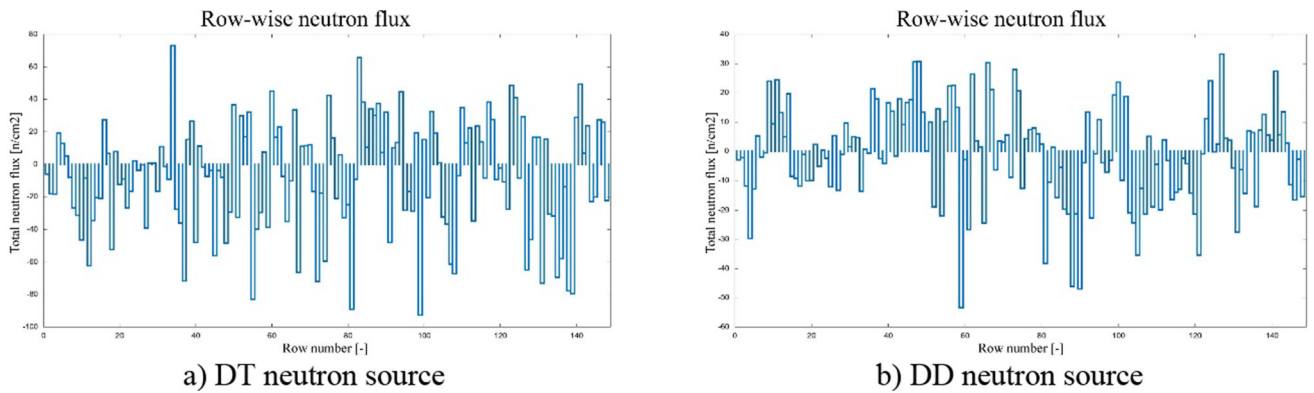
Fig. 14 Row-wise neutron flux at detector—the sodium defect—direct geometry

Fig. 15 Total neutron flux at detector—the sodium defect—rotated geometry

However, this effect seems to be very weak to be usable in real measurement.

3.4 Sodium defect—rotated geometry

The simulations in rotated geometry were performed for all investigated cases, however, as it is also demonstrated in Fig. 5, no relevant results were obtained. Some patterns in detector responses were observable, but we judged them not applicable in a real industrial environment, specially if direct geometry brought relevant responses. It should be noted, that in the case

of the multigroup calculation, patterns were identified. After investigation, we have revealed that these patterns were artificial and caused by the discrete energy groups structure (Fig. 15).

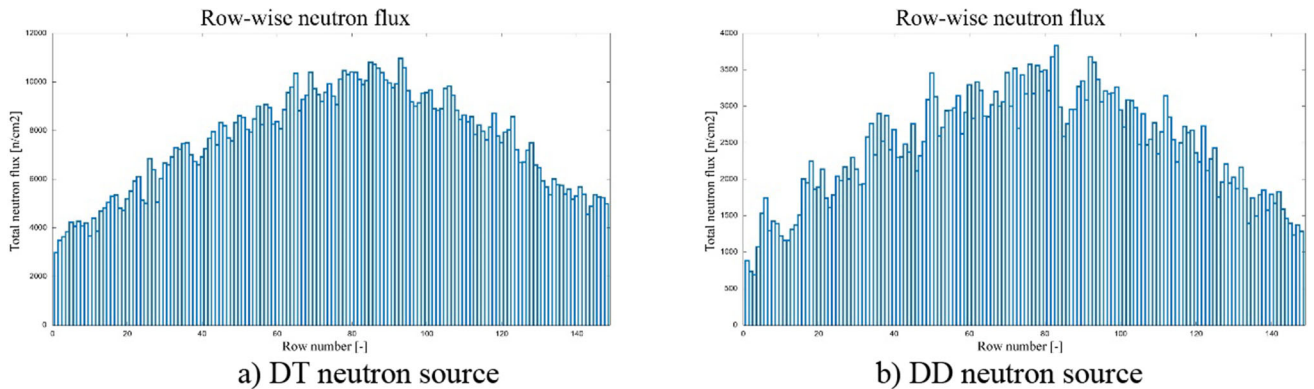### 3.5 Overheated steam defect—direct geometry

As found in the water defect simulations, neither use of DT nor DT source enabled the proper identification of the related rupture. To change the slowing down properties of secondary media (also affecting absorption of

1654

Eur. Phys. J. Spec. Top. (2023) 232:1645–1656
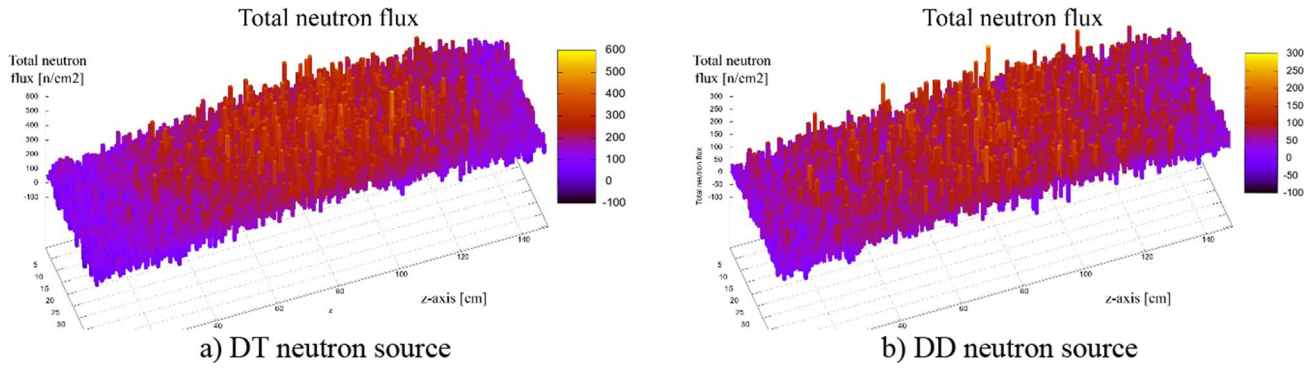
Fig. 16 Total neutron flux at detector—the steam defect—direct geometry
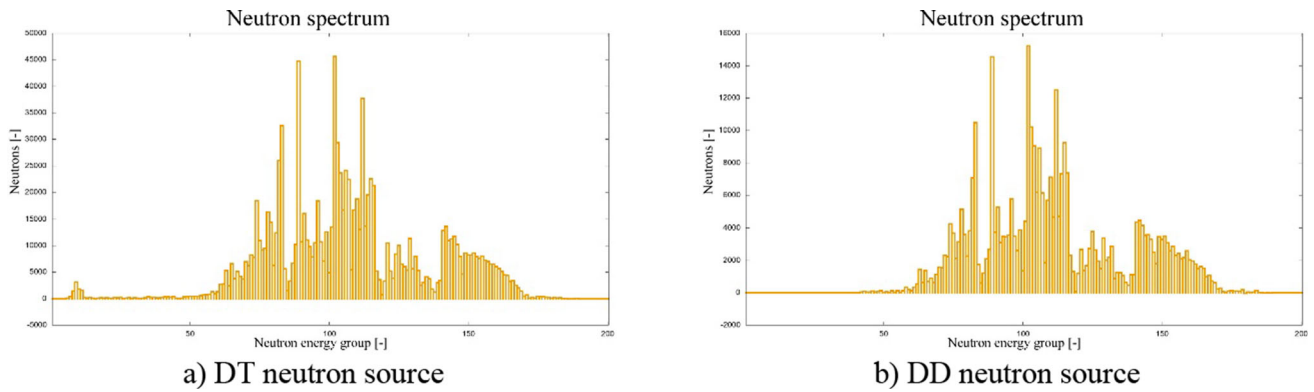
Fig. 17 Neutron spectrum at detector—steam—direct geometry

Fig. 18 Row-wise neutron flux at detector—the steam defect—direct geometry

neutrons), the overheated steam was used as the backfilling media. The results are shown in Figs. 16, 17, 18.

As can be seen in Fig. 16, the pattern can be easily recognized in the detector responses for the DT and DD neutron sources. Again, the response pattern is sharper in the case of the DT source. Interestingly the neutron spectra over the detector presented in Fig. 17 is almost identical with exception of the fast neutron peak in the case of the DT source.

The row-wise neutron fluxes presented in Fig. 18 suggest the good detectability of the rupture, where shorter irradiation time can be needed for the DT source.

4 Conclusions

In general, non-destructive testing is capable of detecting defects of safety-related industrial components, where a failure could pose a significant hazard and cause severe economic losses. Currently, imaging techniques

utilizing gamma or X-ray sources are mainly used, but for industrial-sized large components, these methods usually fail. The utilization of neutrons in radiography is a promising alternative, especially for industrial applications, but significant scientific progress is needed to utilize the advantages of fast neutrons in the real industrial environment. The paper focuses on printed circuit heat exchangers, which are promising large industrial components, with a potential for application in Generation IV nuclear reactors. Other authors showed that the PCHE can be controlled in the production facility by DT source and film detector. However, during outage and maintenance activities, the ruptures on the level of one plate need to be timely revealed. The results obtained with the simplified model demonstrated the relevant potential of the fast neutron radiography and PCHE for sodium fast reactors. The direct geometry and DT neutron source in conjunction with the proposed evaluation principle from detector responses enables the detection of the rupture on sodium side. On the other hand, the backfilling the secondary channel with overheated steam (or other media with similar hydrogen content) allows the detection of defects on the secondary side of the exchanger. Here both DT ad DD sources showed promising results. The rotated geometry did not confirm its usability. Moreover, the simulations performed confirmed the necessity of the use of continuous libraries, where the multigroup approach significantly altered the detector responses. The next steps of the research team will be focused on the more precise simulations considering real beam collimators and the response functions of the detectors available on the market. In addition, to validate our simulations, the simplified mock-up of the PCHE will be constructed and real irradiation utilizing the Tandetron accelerator in Piešťany (which belongs to the Slovak Academy of Sciences) will be performed in near future.

Data availability statement All data generated or analysed during this study are included in this published article.

References

1. International Atomic Energy Agency, *Training Guidelines in Non-destructive Testing Technique* (IAEA, Vienna, 2013)
2. N. Bartel, M. Chen, V.P. Utgikar, X. Sun, Comparative analysis of compact heat exchangers for application as the intermediate heat. Ann. Nucl. Energy **81**, 143 (2015)
3. S. Aakre, Nuclear code case development of printed-circuit heat exchangers with thermal and mechanical performance testing. In: 6. International Supercritical CO_2 Power Cycles Symposium, Pittsburgh, USA (2018)
4. Heatric, Heatric Printed Circuit Heat Exchangers. https://www.heatric.com/heat-exchangers/. Accessed 15 Aug 2022
5. S. Lee, S. Shin, S. Chung, Evaluation of thermal-hydraulic performance and economics of Printed Circuit Heat Exchanger (PCHE) for recuperators of Sodium-cooled Fast Reactors (SFRs) using CO_2 and N_2 as working fluids. Nucl. Eng. Technol. **54**, 5 (2022)
6. C.-Y. Chang, W.-H. Che, L.H. Saw, A.A. Arpia, Performance analysis of a printed circuit heat exchanger with a novel mirror-symmetric channel design. Energies **14**, 14 (2021)
7. International Atomic Energy Agency, *Neutron Imaging: A Non-destructive Tool for Materials Testing* (IAEA, Vienna, 2008)
8. E. Lehmann, M. Raventos, R. Harti, Methodical progress in neutron imaging at PSI. Phys. Procedia **88**, 250 (2017)
9. A. Tremsin, T. Shinohara, K. Oikawa, J. Li, P. Monteiro, Non-destructive mapping of water distribution through white-beam and energy-resolved neutron imaging. Nucl. Instrum. Methods Phys. Res. A: Accel. Spectrom. Detect. Assoc. Equip. **927**, 174–183 (2019)
10. A. P. Kaestner, C. Grünzweig, E. H. Lehmann, Challenging non-destructive applications for neutron imaging. In: 18th World Conference on Nondestructive Testing, Durban, South Africa (WCNDT 2012) (2012)
11. Massachusetts Institute of Technology, Printed-Circuit Heat Exchanger (PCHE). https://ase.mit.edu/projects/printed-circuit-heat-exchanger-pche/. Accessed 10 June 2022
12. N. Kardjilov, I. Manke, A. Hilger, M. Strobl, J. Banhart, Neutron imaging in materials science. Mater. Today **14**, 6 (2011)
13. R. Pöllännen, T. Sisskonen, Detection of fast neutrons from shielded nuclear materials using a semiconductor aspha detector. Appl. Radiat. Isot. **90**, 187 (2014)
14. D. Greiffenberg et al., Detection efficiency of ATLAS-MPX detectors with respect to neutrons. Nucl. Instrum. Meth. A **607**, 38 (2009)

1656

Eur. Phys. J. Spec. Top. (2023) 232:1645–1656

15. A.V. Chernykh et al., Fast neutron detector based on surface-barrier VPE GaAs structures. JINST **10**, C010121 (2015)

16. C. Lynde et al., Demonstration of coded-aperture fast-neutron imaging based on Timepix detector. Nucl. Instrum. Methods Phys. Res. A Accel. Spectrom. Detect. Assoc. Equip. **954**, 161373 (2020)

17. A. Šagátová et al., Semi-insulating GaAs based detector of fast neutrons produced by D-T nuclear reaction. J. Instrum. **11**, 12 (2016)

18. D.S. McGregor et al., Thin-film-coated bulk GaAs detectors for thermal and fast neutron measurements. Nucl. Instrum. Methods Phys. Res. A Accel. Spectrom. Detect. Assoc. Equip. **466**, 21 (2001)

19. Medipix, Medipix Colaboration. https://medipix.web.cern.ch/medipix2. Accessed 17 Mar 2922

20. A.S. Tremsin, J.V. Vallerga, Unique capabilities and applications of Microchannel Plate (MCP) detectors with Medipix/Timepix readout. Radiat. Meas **130**, 106228 (2020)

21. A. Šagátová et al., Semi-insulating GaAs detectors degraded by 8 MeV electrons up to 1500 kGy. J. Instrum. **16**, C12032 (2021)

22. W.A. Wieselquist, R.A. Lefebvre, M.A. Jessee (eds.), *SCALE code system, ORNL/TM-2005/39, version 6.2.4* (Oak Ridge National Laboratory, Oak Ridge, 2020)

23. B. Vrban, F. Osuský, V. Nečas, *Effective dose Calculation in the VVER-440 Maintenance Area, Transactions of the American Nuclear Society* (American Nuclear Society, Illinois, 2020)